AIAA-2002-1062

Compressibility Effects on the Growth and Development of Large-Scale Structures in an Axisymmetric Jet

B. Thurow, J. Hileman, M. Samimy and W. Lempert

The Ohio State University
Department of Mechanical Engineering
Columbus, OH 43210

40th Aerospace Sciences Meeting & Exhibit
January 14 -17, 2002/ Reno, NV

COMPRESSIBILITY EFFECTS ON THE GROWTH AND DEVELOPMENT OF LARGE-SCALE STRUCTURES IN AN AXISYMMETRIC JET

B. Thurow*, J. Hileman*, M. Samimy† and W. Lempert‡

The Ohio State University
Gas Dynamics and Turbulence Laboratory
Department of Mechanical Engineering
Columbus, OH 43210

A temporally resolved flow visualization system that produces 17 flow images over a time span of 128 microseconds is used to visualize the mixing layers of a Mach 1.28 (M_c=0.59) and a Mach 2.06 (M_c=0.87) ideally expanded high Reynolds number axisymmetric jets. These image sequences revealed details about the effects of compressibility on the dynamics of turbulence structures. In general, the observations made in the axisymmetric jets are similar to observations made in planar shear layers at similar convective Mach numbers. Large-scale structures progressively become more three-dimensional and less organized with increasing compressibility and are more difficult to identify and track in the Mach 2.06 jet. Furthermore, while specific examples of 'tilting', 'stretching', 'tearing' and 'pairing' are demonstrated in a single image sequence obtained in the Mach 1.28 jet, these processes are less pronounced in Mach 2.06 case. Spatial correlation functions are used to extract quantitative information about the size, shape and convective velocity of large-scale structures in these flows. The ensemble average convective velocity of the Mach 1.28 jet was 270 m/sec, which is higher than the theoretical prediction of 206 m/sec. The histogram of the convective velocity, however, revealed a broad distribution of convective velocities. The Mach 2.06 jet, on the other hand exhibited a bimodal ensemble average convective velocity distribution with a 'fast' mode at ~420 m/sec and a 'slow' mode at ~180 m/sec. The histogram showed almost Gaussian distributions centered around both the fast mode and the slow mode. These modes are equally spaced from the theoretical convective velocity of 303 m/sec. Approximately 2/3 of the measured velocities were in the slow mode.

Introduction

The understanding of the dynamic behavior of compressible flows has long challenged researchers, as the nature of turbulence structures becomes more complicated and perplexing than in incompressible flows. This change in turbulence characteristics has some very profound effects on the flow, the most noted being a major reduction in the shear layer growth rate.

In order to categorize this effect, a non-dimensional parameter, the convective Mach number, was introduced.[1,2] For two pressure-matched parallel streams with equal specific heats this parameter is given as:

$$M_c = \frac{U_1 - U_2}{a_1 + a_2} = \frac{U_1 - U_{c,i}}{a_1} = \frac{U_{c,i} - U_2}{a_2} \quad (1)$$

where U_1 and U_2 are the high- and low-speed free stream velocities, a_1 and a_2 are the speeds of sound and $U_{c,i}$ is the theoretical isentropic convective velocity. [This number was originally intended to represent a reference frame moving at U_c, the convective velocity of large-scale turbulence structures contained within the shear layer. Recent experiments, however, have shown that structures do not convect at the speed indicated in equation 1.[3-12] Despite the deviation of the actual convective velocity from the theoretical value obtained in Equation 1, the convective Mach number is still commonly used as a parameter to represent the degree of compressibility.

The role of compressibility in the formation and development of structures has been experimentally studied using flow visualization in planar shear layers[1-3,5-8,10,13,23,25], base flows[9,28] and jets[4,11,12,14]. For M_c<0.5, the turbulence structures are similar to the incompressible structures observed by Brown and Roshko[15]. They are highly two-dimensional, organized and coherent and appear as large spanwise rollers.

* Graduate Student, AIAA Member
† Professor, AIAA Associate Fellow; Corresponding author
‡ Associate Professor, AIAA Associate Fellow

Events such as pairing are commonly seen and easy to follow. For $0.5<M_c<1.0$, three-dimensionalities begin to dominate and turbulence structures can no longer be defined by their spanwise coherence as they become increasingly more three-dimensional and less organized, thus making them more difficult to identify. Events such as pairing are not as clear and become much more difficult to observe. For $M_c>1.0$, turbulence structures are fully three-dimensional with very little resemblance to their incompressible counterpart. Furthermore, linear stability analyses[16,17] indicate the emergence of 'fast' and 'slow' modes as the primary instabilities in the flow.

One parameter of interest to researchers is the convective velocity of structures. This parameter can conveniently be measured using multiple image flow visualization techniques such as double-pulse PLIF and high-speed cinematography. Experiments performed predominantly on planar shear layers as well as on base flows and jets have indicated a significant deviation of the convective velocity from its theoretical isentropic value. This deviation has appeared as either a 'fast' or a 'slow' mode and has led to the stream selection rule that states that for a supersonic/subsonic stream combination, the convective velocity will err closer to the high-speed stream while for a supersonic/supersonic combination the velocity will err to the lower speed stream.

The majority of compressibility effects discussed above have been based on observations in planar shear layers. In general, these observations have translated well to other flow configurations such as base flows and jets. However, it remains to be seen what differences might arise due to a change in flow geometry. In this paper, compressibility effects on axisymmetric jets are studied using a temporally resolved flow visualization technique, which yields 17 time-resolved images. Spatial cross-correlations are used to objectively track spatial features of the flow through the sequence of images and to obtain more details concerning the size, shape and convective velocity of structures within an axisymmetric jet.

Facility and Equipment

All of the experiments were conducted at The Ohio State University's Gas Dynamics and Turbulence Laboratory (GDTL). The facility consists of a jet stand and stagnation chamber to which a variety of nozzles may be attached. Air is supplied to the stagnation chamber from two four-stage compressors; it is filtered, dried and stored in two cylindrical tanks with a total capacity of 42.5 m^3 at 16.5 MPa (1600 ft^3 at 2500 psi). The stagnation chamber contains a perforated plate and two screens of varying porosity to condition the flow to be as uniform as possible prior to entering the nozzle. The facility has been described in more detail elsewhere.[18,19]

Two jet nozzles were used in this study that have design Mach numbers of 1.3 and 2.08. The nozzles have a 25.4 mm exit diameter with the expansion contour designed using a computer program based on the method of characteristics with the stipulation of uniform flow at the nozzle exit. The Mach 2.08 nozzle had a lip thickness of <1 mm and the Mach 1.3 nozzle a slightly thicker lip of 2.5 mm. The nozzle Mach numbers were experimentally determined using a pitot probe to be 1.28 and 2.06, respectively. The jets exhaust into a large room that can also serve as an anechoic chamber and exits the facility through a large bell-mouth at the opposite end of the chamber. Pressure to the stagnation chamber is controlled manually through the actuation of a Fisher control valve and can be maintained at constant pressure within 0.1 psi. Pressure was set for an ideally expanded flow and held constant through each set of experiments.

Experimental Diagnostics

A pulse burst laser and an ultra high-speed CCD camera were used to take sequences of 17 time correlated flow visualization images. The pulse burst laser has been described elsewhere[12,20-22] and only a short description will be provided here. The laser is a custom built 2nd generation Nd:YAG laser system that achieves a high repetition rate through the use of a dual Pockel's cell arrangement. The output is frequency doubled at 532 nm (green). The laser can create between 1 and 99 pulses over a time span of approximately 125 microseconds and can operate at a maximum rate of 1 MHz. Due to camera limitations the laser was set to generate 17 pulses. In order to use the full time range of the burst of pulses, pulse spacing was set to 8 microseconds. Each pulse is 10 nsec in duration and contains an average of 5 mJ per pulse. The overall repetition rate of the system is 10 Hz.

For flow visualization, the laser beam was formed into a sheet and was directed through various slices in the flow field. Seeding was provided using product formation where water contained in the warm moist ambient air condensed upon entrainment into the jet and mixing with the cold and dry air of the jet core. Concerns about the size of the particles formed and the response time of their formation have been previously addressed, and the particles are believed to accurately mark the features of the shear layer.[23] Laser light scattered from the condensed water particles was then captured and recorded using a Dalsa 64K1M 12-bit CCD camera. This camera can capture 17 images with a resolution of 248 x 248 pixels at a rate up to 1 MHz.

Due to the masking technique used to create the high frame rate, the fill factor of the camera is on the order of 3% with an effective pixel size ~ 10 microns. Despite this limitation of the camera's sensitivity, the combination of the laser and camera is still sufficient to visualize the flow.

Description of Experiments

The temporally resolved flow visualization system was used to visualize both streamwise and cross-stream planes of Mach 1.28 and Mach 2.06 axisymmetric free jets. The convective Mach numbers are 0.59 and 0.87 respectively. As such, the Mach 1.28 jet is expected to be slightly compressible while the Mach 2.06 jet is expected to be fully compressible.

For the streamwise image sequences, three areas of the jet were examined: near the nozzle exit, near the end of the potential core and downstream of the potential core. The length of the potential core was estimated from an equation given by Murakami and Papamoschou[24] to be 7.3 and 10.6 jet diameters for the Mach 1.28 and 2.06 jets, respectively. The measured potential core for the Mach 1.28 jet was about 6 jet diameters.[18] The visual length of the potential core is slightly longer as the seed particles do not mark the entire width of the mixing layer. Cross-stream cuts were taken at x/D locations of 3, 6, 9, 12 and 15.

In this paper, the streamwise images taken near the end of the potential core are the primary focus. The remaining data will be analyzed in further detail elsewhere and is only referred to in this paper to complement the results of the streamwise images.

For the Mach 1.28 nozzle, data from an earlier experiment with pulse spacing of 10 microseconds was used. The streamwise images span from ~ 4.25 to 10.6 jet diameters. For the Mach 2.06 jet, the streamwise images spanned from ~ 5.25 to 11.75 jet diameters downstream of the nozzle exit. Over 17 frames, each sequence of images covers a non-dimensional time of approximately 2.0. The non-dimensional time, τ, is defined as:

$$\tau = \frac{U_{c,i}\,\Delta t}{\delta_{local}} \qquad (2)$$

where $U_{c,i}$ is the theoretical isentropic convective velocity calculated from equation 1, Δt is the time separation between the first and last frame and δ_{local} is the local shear layer thickness. The shear layer thickness was determined by analyzing an ensemble average of 100 flow visualization images. The location where the intensity in the mixing layer reaches 25% of its maximum value was used as the cutoff point. The shear layer thickness was determined at x/D=5.5 for the Mach 1.28 jet and at x/D=8.0 for the Mach 2.06 jet. This x/D location corresponds to 75% of the potential core length for each case, respectively.

Digital Image Processing and Analysis

Before images were analyzed, an average background image was subtracted from each image. Images were then corrected on a shot-to-shot basis for non-uniformity of the laser sheet intensity and then a 3x3 pixel low-pass filter was applied in an attempt to remove 'speckle' noise while preserving the large-scale structure information. This has also been shown by Wainner and Seitzman[25] to generally improve the success of cross-correlations in tracking structures. Images were then scaled to have values ranging between 0 and 1. Following this preprocessing, image sequences were saved in a movie format for viewing.

In order to objectively characterize the large-scale turbulence structures contained within the mixing layer, spatial correlations and space-time cross-correlations were performed on the image sequences. For both of these processes, large-scale turbulence structures within the jet had to be identified. In the past, structures have been identified both manually and automatically. We have chosen to use an automated method for both its objectivity in selecting a structure and ease in processing large data sets. In this automated method, a window is positioned along the centerline of either side of the mixing layer at some prescribed streamwise location and its width and height determined by the local shear layer thickness. The spatial pattern of the mixing layer's intensity within the window is then defined to be the large-scale structure, or 'feature', of interest. It is emphasized that this method of identification has no set criteria for identifying a structure, but arbitrarily defines a structure as the pattern of the fluid that happens to be captured in the window. Earlier results on a Mach 1.3 jet have shown that the convective velocity does not greatly depend on the initial selection of a structure.[26]

Using the convective velocity algorithm to be described later, the effect of the window's streamwise location and size was examined. The average convective velocity was not significantly affected in a 3-4 jet diameter region near the end of the potential core by either the window's size or streamwise location as long as the window was placed upstream of the potential core. The histogram data of the convective velocity was altered slightly by the choice in window size, but the overall features of the histogram remained the same. It was also concluded, in agreement with the results of Smith and Dutton[27] that a window longer in the streamwise direction than it is in the transverse direction generally yields more consistent results.

For these experiments, the optimal window size was determined to be $3\delta_{local}$ wide x 1.5 δ_{local} tall. This

corresponded to a window size of approximately 76 x 38 pixels and spanned the entire mixing layer in the transverse direction. For the results to follow, the windows were centered at x/D=5.5 for the Mach 1.28 jet and x/D=8.0 for the Mach 2.06 jet. For both jets, the x/D position is approximately 75% of the potential core length. Thus, equivalent regions within the jet are being examined. Upon selecting a structure, certain statistical properties of the structure were measured and recorded. These values include the centroid location, area, angle of inclination, and eccentricity of the structure. These values were calculated by converting the structure to a binary image based on a 0.5 threshold and using built-in Matlab routines for determining image statistics.

For any single instantaneous image, the spatial correlation function can reveal information concerning the general shape and size of structures within the flow. The spatial correlation is determined by taking the structure of interest, S, and correlating it with the entire image from which it was taken, I. Both the structure, S, and the image, I, are distinguished from the average intensity signal by subtracting the average structure ($S' = S - \langle S \rangle$) and image ($I' = I - \langle I \rangle$) before calculation. The spatial correlation is then defined as:

$$R(\Delta x, \Delta y) = \sum_{mxn} S'(x, y) I'(x + \Delta x, y + \Delta y) \quad (3)$$

where Δx, Δy are the horizontal and vertical displacements of the structure relative to the image, respectively, and are varied to span the entire image. This value is then normalized so that it takes the value 1.0 for perfect correlation (i. e. when it is correlated with itself) and –1.0 for perfect anti-correlation. In this sense, the identified structure is correlated with the entire mixing layer in order to obtain information about the structure's size, eccentricity and inclination. An ensemble average of many such realizations should yield the average quantities of the structures.

The identified structure from the first image can also be cross-correlated with the remaining 16 images in the image sequence in order to extract a convective velocity. The cross-correlation is given as:

$$R_i(\Delta x, \Delta y) = \sum_{mxn} S_1'(x, y) I_i'(x + \Delta x, y + \Delta y) \quad (4)$$

where the subscript i indicates which image in the sequence is being analyzed. Note that for i=1, the cross-correlation is equal to the spatial correlation just described. The cross-correlation is also normalized so that it takes values between –1.0 and 1.0. In this fashion, a total of 17 cross-correlation matrices are found for each image sequence. In the first matrix, R_1, the maximum correlation will be 1.0 and located at (x_o, y_o, t_1=0) which corresponds to the chosen structure aligning right on top of itself. In the second correlation matrix, R_2, the maximum correlation level will drop below 1.0 and be located at a new position ($x_o+\Delta x_{1\to2}$, y_o, $t_2 = t_1+\Delta t_{1\to2}$), where $\Delta x_{1\to2}$ represents a shift of the peak in the streamwise direction and $\Delta t_{1\to2}$ indicates the time delay between images. A transverse movement of the structure, Δy, is also allowed, but typically negligible. This trend should continue for each subsequent correlation until at some time, t_{last}, the structure will no longer be identifiable. This process will result in an array of structure location shifts, **x**, and an array of times, **t**, which can be plotted on an x-t diagram. The slope of a linear fit through these points will be the convective velocity. Using the least squares method to fit a line through these points, it is easy to show that the convective velocity is:

$$U_c = \frac{(\mathbf{x}, \mathbf{t})}{(\mathbf{t}, \mathbf{t})} \quad (5)$$

where (,) is the inner product. This process of calculating convective velocity can be performed on both ensemble averages of the correlation matrices or on individual image sets. For the ensemble averages, an accurate average convective velocity of structures will be calculated. For instantaneous realizations, a histogram of convective velocities can be determined.

In the case of tracking a structure in an individual set of images, a single well-defined peak in the correlation matrix should mark the location of a structure. However, the structure might evolve to such an extent that it cannot be identified through an entire sequence of images. To overcome this challenge, an algorithm was developed to distinguish peaks that correspond to the desired structure from peaks that are the result of other features in the flow. The algorithm is designed only to look for peaks locations that are physically possible. This is accomplished by only looking at correlation peaks with a streamwise location that corresponds to a convective velocity that is positive and does not exceed the jet exit velocity. If the program could not identify a peak within these limits, the loop was stopped and the next image sequence was examined. Therefore, some velocity calculations may not be based on the full set of 17 images. Two criteria for accepting or rejecting convective velocity measurements was also used. The first criterion was set so that a one pixel deviation in the measured location of the last identifiable peak would correspond to a velocity change of less than 10 m/sec ($\Delta x_{1\to last}/\ \Delta t_{1\to last} < 10$). The second criteria examined the deviation of the x-t coordinates from the least-squares fit. An appropriate method for applying this criterion is still being determined and currently only the most apparent errors are being eliminated. By changing this error limit, the overall results initially appear to be insensitive to this parameter.

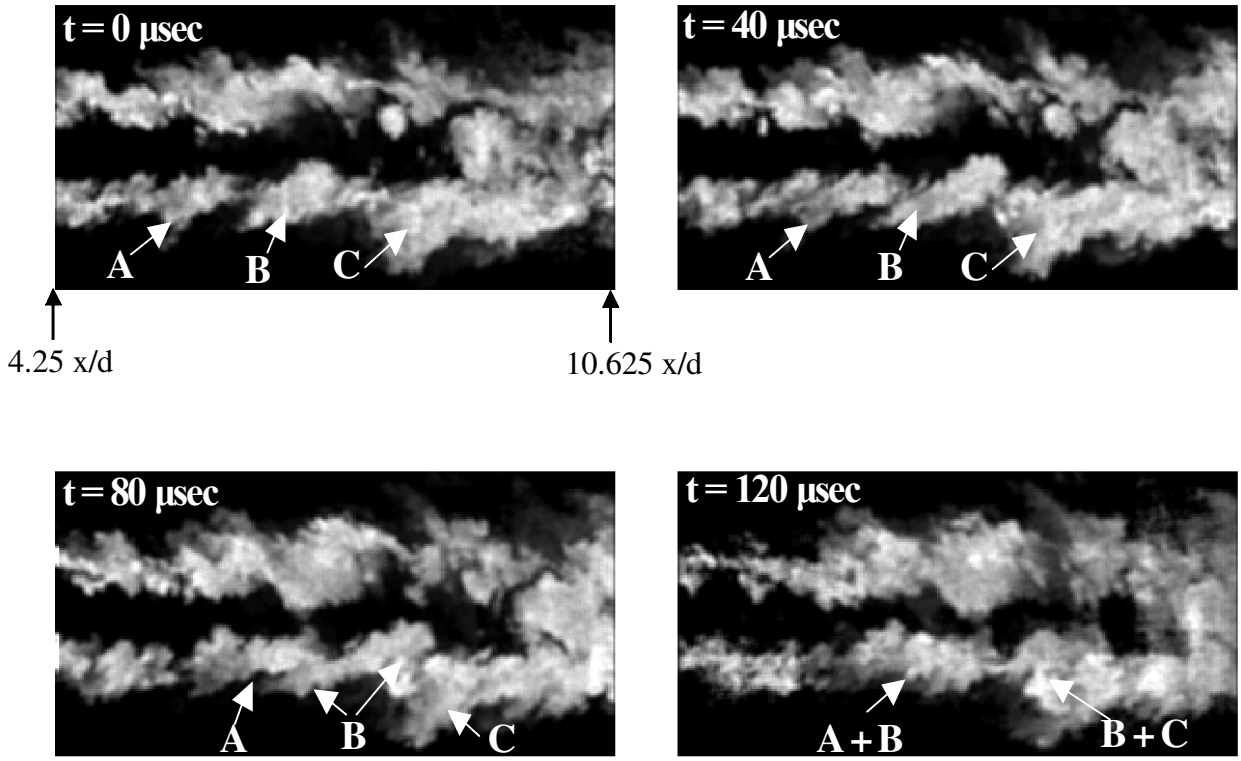

Figure 1 – Temporally resolved flow visualization images of a Mach 1.28 (M_c=0.59) axisymmetric jet.

Results and Discussion

Temporally Resolved Flow Visualization:

Figure 1 is a sequence of 4 images taken of the Mach 1.28 (M_c=0.59) jet. Flow is from left to right and the bright regions correspond to areas where moisture in the entrained ambient air into the mixing layer has condensed. Thus, only the mixing layer is being visualized. The analysis of the images in Figure 1 is greatly aided by the addition of 13 other frames that can be played in a movie format. The movie format makes the development and interaction of structures within the mixing layer much easier to visualize. As seen in this image (particularly in the upper half of the mixing layer in the 3rd image) and previously reported results[12,26] one observes only the occasional appearance of structures that resemble the familiar core and braid region associated with structures in incompressible shear layers. These structures do not appear to be globally organized with respect to other structures in the shear layer as they do in incompressible shear layers. Furthermore, the superposition of many smaller scales is evident by the jagged edges at the high- and low-speed boundaries of the mixing layer. Cross-stream image sequences (not shown here) reveal that the turbulence structures are quite three-dimensional. Streamwise vortices are also deemed to play a key role in the development of the mixing layer as inferred by the large swirling motions of fluid observed in the cross-stream movies. These overall observations agree quite well with the observations made in studies of planar shear layers.

The technique used here provides some additional insights concerning the evolution and mechanisms of interaction between structures. Figure 1 depicts an event that typifies the dynamics of structures in a compressible mixing layer. In the first frame, three structures are identified and labeled as ‘A’, ‘B’ and ‘C’. These structures do not appear to be the same as structures seen in incompressible flows, but distinguish themselves from the rest of the mixing layer and are separated by small braid-like regions. In the second frame (which is really the 5th in the full sequence of images), structures ‘A’ and ‘B’ are slightly tilted and stretched in the direction of the shear. Structure ‘C’, meanwhile, appears roughly the same as it did in frame 1, possibly tilting and stretching slightly. In the third frame (9th in the full sequence) structure ‘B’ is dramatically tilted and stretched from its original shape and now overlaps ‘A’ on the low-speed side of the mixing layer and ‘C’ on the high-speed side. In the fourth frame (13th in the full sequence), no evidence of

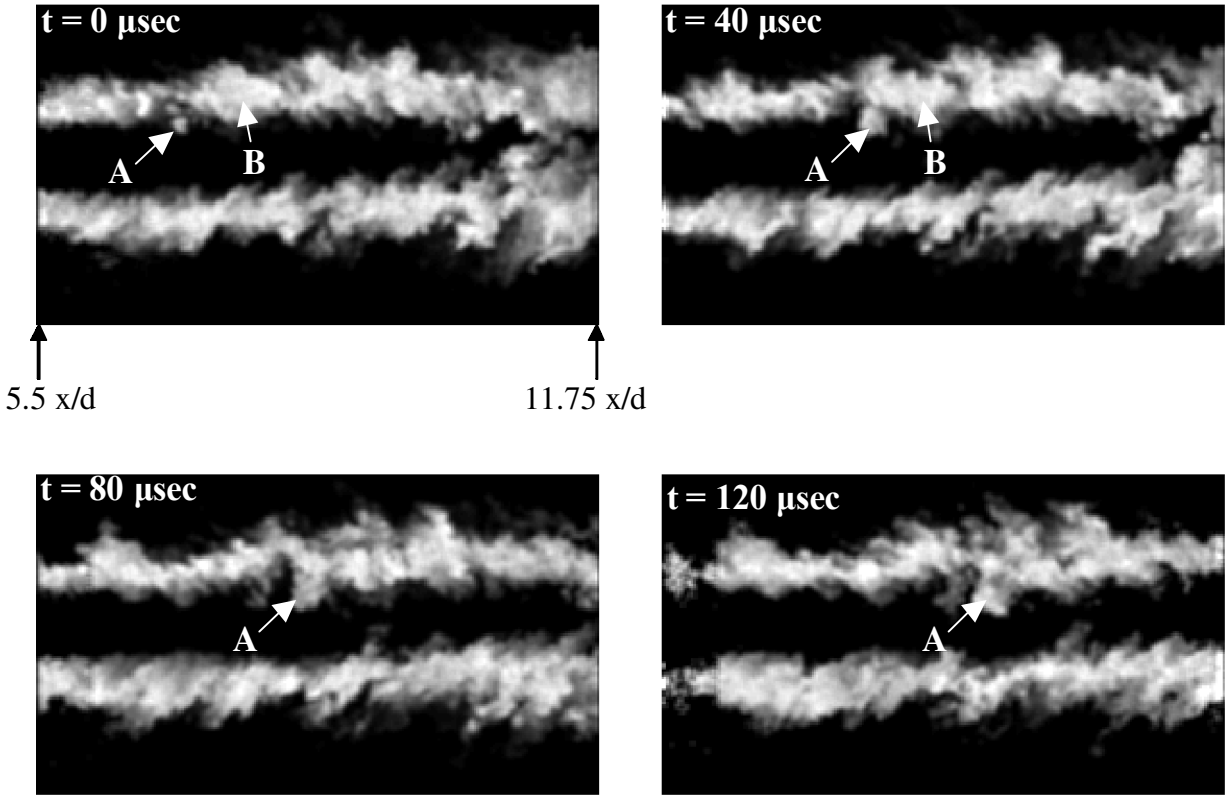

Figure 2 – Temporally resolved flow visualization images of a Mach 2.06 (M_c=0.87) axisymmetric jet.

structure 'B' exists as it has been torn apart by the pairing interaction with 'A' and 'C'. Two identifiable structures remain that are labeled 'A+B' and 'B+C' to indicate their origin. The developments characterized in Figure 1 can be generalized and decomposed into the basic processes of 'tilt', 'stretch', 'tear' and 'pair'. After viewing hundreds of movies, it is quite clear that these processes demonstrated in Figure 1 are very common and take place throughout the mixing layer on a wide variety of scales and occurrence. Only experimental techniques such as this could reveal the nature of this rapid development of structures and could help in clarifying the mechanisms responsible for the growth and destruction of a turbulent structure.

Figure 2 shows four images (out of a sequence of 17) that are typical for the Mach 2.06 (M_c=0.87) jet. Some of the features observed in the M_c=0.59 case are still observed, but also some major differences observed. For example, a structure is marked 'B' in the first frame, which appears to be connected to the structure just upstream of it by a thin braid-like region of fluid. This structure, however, is not as distinct as structures seen in Figure 2 and evolves much more rapidly as it is difficult to identify it beyond the second frame. The tilting, stretching, tearing and pairing events depicted in Figure 1 also occur quite often, but are more difficult to follow in still images as the structures undergoing the processes are not as easy to identify and the events appear to happen more rapidly. As in the Mach 1.28 case, cross-stream image sequences indicate the presence of streamwise vortices through the large swirling motions that are observed in the mixing layer.

The image sequences also reveal more details concerning the three-dimensional nature of structures. Namely, many of image sequences show the appearance of fluid from out of the page. This is demonstrated by the fluid structure marked 'A' in the images. In the first image, this fluid appears as a small patch of fluid detached from the rest of the mixing layer. As the flow progresses, this fluid element appears to grow in size to the point that in the last image, one would not be able to recognize that this fluid came from out of the plane. It is interesting to note that a manual measurement of this feature's velocity is approximately 440 m/sec. It cannot be determined from these images whether the growth of structure 'A' is an actual growth of a structure or if it results from the passing of a structure with an azimuthal as well as a longitudinal motion through the imaging plane. This

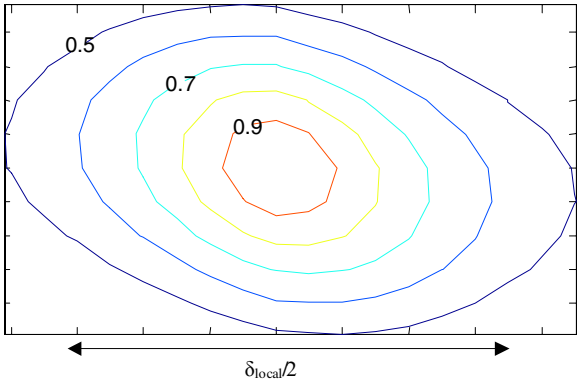

Figure 3 – Spatial correlation for Mach 1.28 axisymmetric jet.

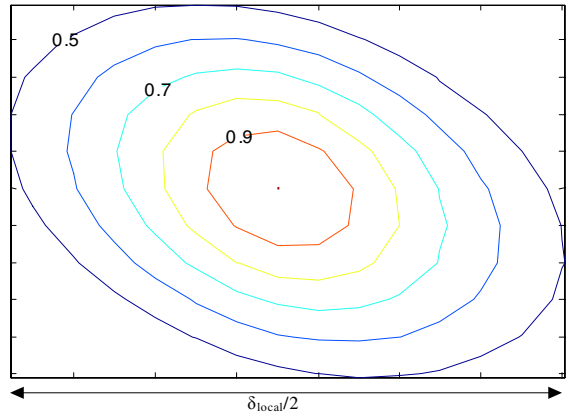

Figure 4 – Spatial correlation for Mach 2.06 axisymmetric jet.

type of motion, however, is much more common in the Mach 2.06 jet than it is in the Mach 1.28 jet. This does demonstrate, however, the inherent change in structures from two-dimensional rollers to highly dynamic three-dimensional structures. As in the M_c=0.59 case, these observations agree well with observations made on planar shear layers.

Spatial Correlations:

Spatial correlations of structures in the mixing layer should reveal some details concerning structure size and shape within the mixing layer. Figures 3 and 4 are ensemble averages of the spatial correlation matrix for the Mach 1.28 and 2.06 jets, respectively. A total of 250 image sets were averaged for Mach 1.28 case and 100 for the Mach 2.06 case. Both figures are for structures in the upper half of the mixing layer and thus the high-speed fluid side is in the bottom of the plots. Generally, the 0.5 contour line has been used to make measurements on the eccentricity and angle.[27,28] For the Mach 1.28 jet, the eccentricity is 0.85 indicating a fairly eccentric shape. Furthermore, the angle of the major axis relative to the streamwise direction is ~8 degrees. The 0.5 contour of the Mach 2.06 jet is slightly less eccentric at 0.77 and not as inclined toward the streamwise direction or major axis (~24 degrees).

These results are contrary to what one might expect to happen if the structures were primarily of the roller type seen in incompressible flows. In the incompressible case, one would expect to see the structures become more and more inclined towards the streamwise direction with increasing convective Mach number. The opposite trend observed here is felt to be a product of the change in the nature of structures from two-dimensions to three-dimensions. The spatial correlation contours have not yet been examined for various window sizes and locations, which might reveal more details about the development of structures as they progress in the mixing layer. Therefore, more work is needed before any conclusive statements can be made regarding the spatial correlations.

Cross-correlation / Convective Velocity Results:

We will first examine the ensemble average cross correlation results. For each case, there are 17 images similar to Figures 3 and 4 from which a peak location can be identified as the location of the average moving structure. As opposed to showing all 17 two-dimensional contour plots, however, it is more convenient to only show the correlation level as it varies in the streamwise direction (one dimension). Figure 5 is a graph of the correlation level for select time separations in the Mach 1.28 jet. As expected, the maximum correlation for Δt = 0 µsec is 1.0 and it drops off with increasing streamwise position. For a time separation of 10 microseconds, the correlation level has dropped to about 0.87 and is located about 5 pixels downstream. For increasing time separations, the correlation level drops and the peak broadens. At Δt = 120µsec, the maximum correlation is about 0.35 and the peak is quite broad. If one were to plot the location of this peak on an x-t diagram, the slope of the line fit through these points will be the average convective velocity for the Mach 1.28 jet. This plot is shown in Figure 6. The average convective velocity is determined to be 270 m/sec, which is in agreement with an earlier report of this work.[12,26] This velocity is well above the theoretical prediction of 206 m/sec.

Figure 7 is a plot of the streamwise correlation levels vs. time for the Mach 2.06 jet. A similar trend to

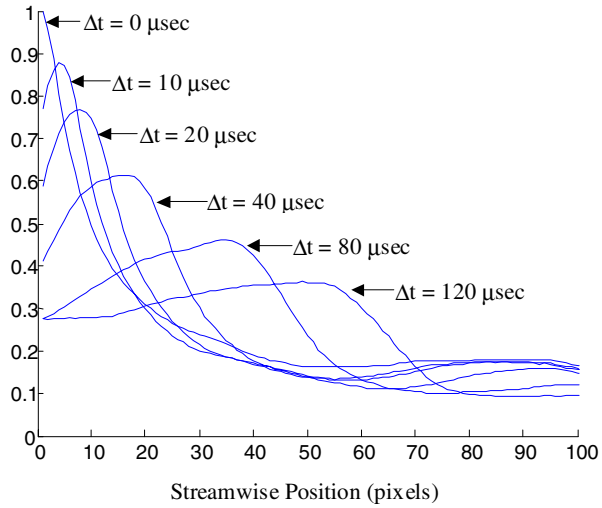

Figure 5 – Streamwise correlation levels for various time separations in a Mach 1.28 axisymmetric jet.

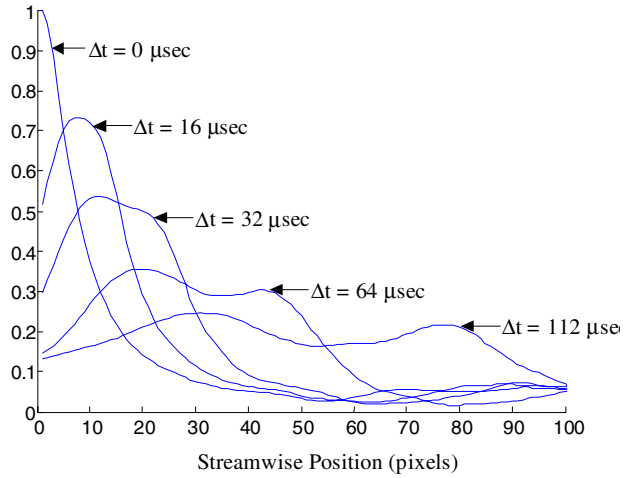

Figure 7 – Streamwise correlation levels for various time separations in a Mach 2.06 axisymmetric jet.

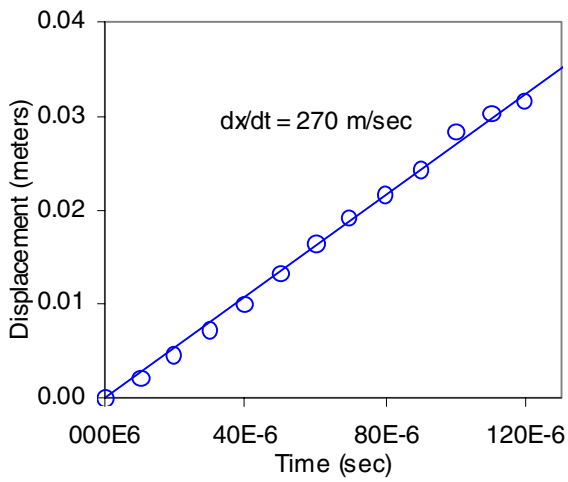

Figure 6 – Plot of peak location vs time for Mach 1.28 axisymmetric jet.

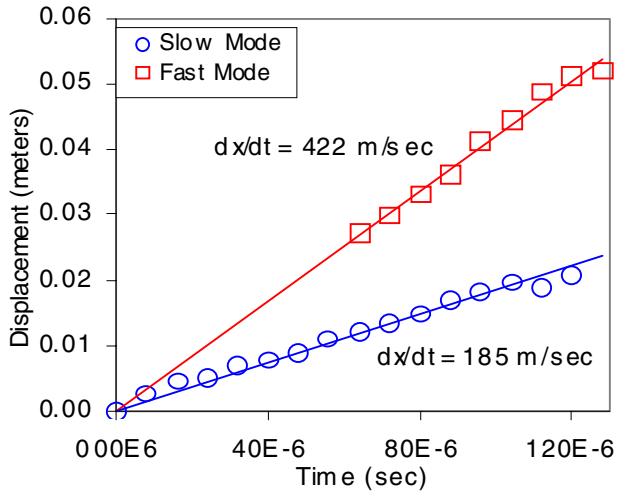

Figure 8 – Plot of peak locations vs. time for Mach 2.06 axisymmetric jet.

the Mach 1.28 case is initially observed as the maximum correlation decreases and the peak becomes increasingly broader. For a time separation of 64 microseconds, however, a very interesting event happens. This broad peak can now be distinctly seen as consisting of two peaks. By individually charting the location of both peaks, two convective velocities can be calculated, a 'fast' mode and a 'slow' mode. This is shown in Figure 8. The points marking the 'fast' mode do not appear until a time separation of 64 The average velocity of the fast mode is 422 m/sec while the slow mode is 185 m/sec. The theoretical value for the convective velocity is calculated as 303 m/sec, which is about halfway between the fast mode and the slow mode. It is worth pointing out that both the fast and slow mode appeared for a variety of window sizes and locations with the average convective velocity not changing by more than 20 m/sec.

Figure 9 is a plot of the correlation levels vs. time for the structures of both jets. The correlation level of structures in the Mach 2.06 jet decrease much more rapidly than for structures in the Mach 1.28 jet, as expected. This is a product of the less robust and more three-dimensional structures that undergo rapid evolution at the higher level of compressibility. Furthermore, the correlation level of the fast mode is slightly below that of the slow mode in the Mach 2.06 jet.

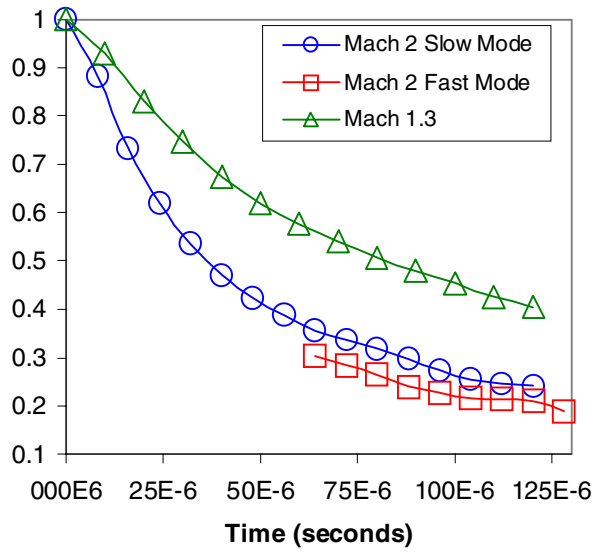

Figure 9 – Correlation level vs. time for Mach 1.28 and 2.06 axisymmetric jets.

Additional details can be obtained about the convective velocity be examining the cross-correlation data for individual image sets, thus getting a histogram of convective velocities. Figure 10 is a histogram of the convective velocity for the Mach 1.28 jet. This data includes structures from both the upper and lower halves of the mixing layer and consists of 320 individual measurements. Approximately 36% of the 500 possible measurements were rejected due to the criteria described earlier. The peak of the histogram is centered around 275 m/sec, which is close to the ensemble average velocity measurement given earlier. There is a broad distribution of velocities, particularly towards the lower velocities. The broad peaks in the cross-correlations in Figure 5 are likely due to this distribution. On average, a structure could be tracked for about 10 frames, or for 1.2 convective time scales. Approximately 25% of the structures could be tracked through all of the frames.

Figure 11 is a histogram of the convective velocities for the Mach 2.06 jet. It consists of 104 individual measurements Approximately 48% of the 200 possible measurements were rejected due to the criteria described earlier.. Clearly, the fast and slow modes observed in the ensemble average data are manifested in the bimodal peaks. These peaks are centered at about 200 and 400 m/sec and are close to the ensemble average values given earlier. Each distribution is nearly Gaussian in shape and appears to be evenly spaced away from the theoretical convective velocity of 303 m/sec. Roughly 2/3 of the measurements are of the slow mode. The change in shape of the histogram was examined for various window sizes. The main features of Figure 11 were largely insensitive to any change in window size. For smaller window sizes, the overall distribution was not as smooth, but distinct peaks still occurred around 200 and 400 m/sec. On average, a structure could be tracked for about 9.5 frames, or for about 1.3 convective time scale. Approximately 15% of the structures could be tracked through all of the frames.

In both cases, individual structure statistics such as centroid location and size were plotted against the convective velocity for that structure. There were no clear trends for any of the cases examined. For the

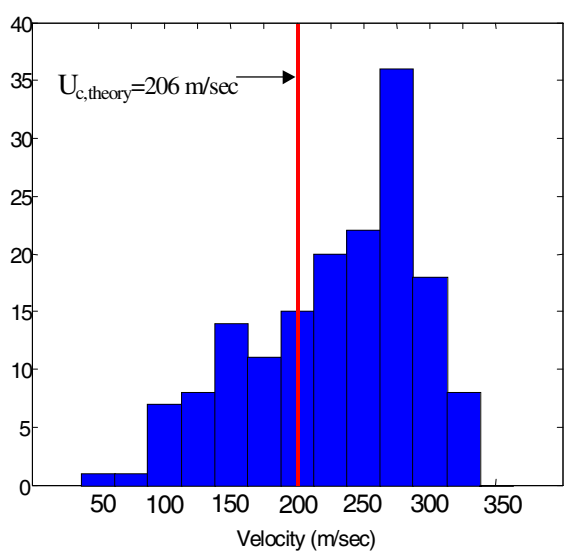

Figure 10 – Histogram of convective velocities for Mach 1.28 jet.

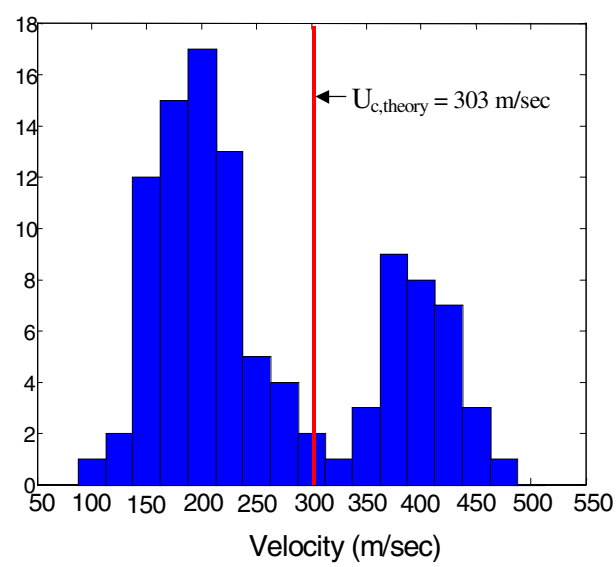

Figure 11 – Histogram of convective velocities for Mach 2.06 jet.

Mach 2.06 case, the transverse centroid location of fast modes was on average only a single pixel closer to the high-speed stream than the slow mode structures. In order to gain more understanding, the ensemble average spatial correlation of all image sequences displaying a fast mode were compared to the ensemble average spatial correlations of image sequences displaying a slow mode. These spatial correlations appeared to be almost identical with the spatial correlation shown in Figure 4. This seems to indicate that the fast and slow mode structures are quite similar to one another. This is an area that needs to be explored in more detail, however.

The convective velocity results presented here are quite unique and worthy of some additional discussion. The deviation of the convective velocity from the theoretical isentropic value was not a surprise and as explained in the introduction has been observed by other researchers and has led to the formulation of the stream selection rule. What is new and surprising about our results, however, is the simultaneous presence of fast and slow modes in the Mach 2.06 jet. All of the convective velocity data conducted in compressible shear layers has indicated the presence of only a single mode.

To address this issue we took a closer look at the convective velocity measurements made in compressible shear layers. The vast majority of these measurements have been conducted on planar shear layers or base flows, both of which are enclosed flows. It is conceivable, that the influence of a solid boundary around the developing shear layer could create a boundary condition that would cause the shear layer to prefer one mode over the other. This mode might then prevent the shear layer from naturally developing into a state with two modes.

It is worth noting that the presence of fast and slow modes has been observed in three-dimensional linear stability analyses of compressible shear layers. These studies by Jackson and Grosch[16] and Day et al.[17] show that for convective Mach numbers greater than 1.0, outer modes of instability waves (fast and slow modes) develop that become more amplified with increasing compressibility. These modes are in addition to the central mode, which dominates at convective Mach numbers below 1.0. Furthermore, the amplification rate of the outer modes does not become significant until convective Mach numbers much greater than the 0.87 in this study. Clearly, however, there is the possibility that these modes are related to observed convective velocities seen here.

Another possible explanation is that the axisymmetric geometry of the jet might allow for the presence of an additional instability mode that is not present or significantly amplified within the planar shear layer. The authors are only aware of two other experimental studies on convective velocity in axisymmetric jets.

Fourgette et al[4] used the same seeding technique used here and two single-pulse Nd:YAG lasers to measure the convective velocity of a Mach 1.5 (M_c=0.7) air jet. Only 36 measurements were made and they had an average of 350 m/sec, which is greater than the theoretical velocity of 230 m/sec for that flow. A histogram of the data was not available, but indications in this work are that the spread in convective velocity measurements is quite significant.

Murakami and Papamoschou[11] utilized a two-laser set-up and PLIF imaging of acetone seeded into a Mach 1.5 jet with co-flow to measure the convective velocity. In this system, the lasers formed adjacent laser sheets that were fired with a specified time delay. Images were subsequently recorded on a single detector. Using both air and helium mixtures, they were able to simulate a variety of convective Mach numbers between 0.43 and 0.72. For each case, only a limited number of measurements were made. In all cases a fast mode was detected with the exception of the lower compressibility results, which matched the theoretical value quite well. There is no indication that a fast and slow mode existed simultaneously. Both of these studies are based on limited datasets and were for convective Mach numbers at or below 0.72. Compared to the convective Mach number of 0.87 in which we observed these modes, the simultaneous modes may not have occurred. More detailed studies are necessary to fully explore these findings.

Conclusions

A temporally resolved flow visualization system was used to visualize and make measurements on two axisymmetric ideally expanded jets. These jets had Mach numbers of 1.28 and 2.06 with respective convective Mach numbers of 0.59 and 0.87. Qualitative flow visualization analysis showed that the behavior of structures in an axisymmetric mixing layer is very similar to the behavior of the well-studied planar compressible shear layer. These flow visualizations also showed further details concerning structure dynamics as tilting, stretching, tearing and pairing events were seen to quite commonly occur in unison in the lower compressibility case. Spatial correlation measurements complement this information, indicating a change in the average structure shape with increasing compressibility.

Cross-correlation measurements of the convective velocity on the Mach 1.28 jet indicate a wide

distribution of velocities with an average velocity of 270 m/sec, which is significantly greater than theoretical velocity of 206 m/sec. Convective velocity measurements on the Mach 2.06 jet showed the simultaneous existence of both fast and slow modes centered around 400 and 200 m/sec respectively. This is equally spaced from the theoretical velocity of 303 m/sec. This trend is observed in both the ensemble averaged cross-correlation data as well as the instantaneous histogram data. Some possible explanations for this dual mode are presented, but ultimately more detailed measurements are necessary to fully explain this effect.

Acknowledgements

The authors would like to thank the National Science Foundation for supporting this research. The first author would like to thank the Department of Defense for his National Defense Science and Engineering Graduate fellowship.

References

[1] Bogdanoff, D. W., "Compressibility Effects in Turbulent Shear Layers," *AIAA. J.* , Vol. 21, 926, 1983.

[2] Papamoschou, D., and Roshko, A., "The Compressible Turbulent Shear Layer: An Experimental Study," *Journal of Fluid Mechanics*, Vol. 197, Dec. 1988, pp. 453-477.

[3] Papamoschou, D., "Structure of Compressible Turbulent Shear Layer," AIAA Paper 89-0216.

[4] Fourgette, D. C., Mungal, M. G., and Dibble, R. W., "Time Evolution of the Shear Layer of a Supersonic Axisymmetric Jet," *AIAA Journal*, Vol. 29, No. 7, 1991, pp. 1123-1130.

[5] Martens, S., Kinzie, K.W., and McLaughlin, D. K., "Wave Structure of Coherent Instabilities in a Planar Shear Layer," AIAA Paper 94-0822, January 1994.

[6] Mahadevan, R., Loth, E., and Dutton, J., "Effect of an Expansion-Compression Wave Pair on Free Shear Layer Dynamics," AIAA Paper 95-0475, January 1995.

[7] Poggie, J. and Smits, A. J., "Large-Scale Coherent Turbulence Structures in a Compressible Mixing Layer Flow," AIAA Paper 96-0436.

[8] Papamoschou, D. and Bunyajitradulya, A., "Evolution of Large Eddies in Compressible Shear Layers," *Physics of Fluids*, Vol. 9, No. 3, 1997, pp. 756-765.

[9] Smith, K. .M., and Dutton, J. C., "Evolution and Convection of Large-scale Structures in Supersonic Reattaching Shear Flows," *Physics of Fluids,* Vol. 11, No. 8, 1999, pp. 2127-2138.

[10] Rossman, T., Mungal, M. G. and Hanson, R. K., "An Experimental Investigation of High Compressibility Non-Reacting Mixing Layers," AIAA Paper 2000-0663.

[11] Murakami, E., and Papamoschou, D., "Eddy Convection in Coaxial Supersonic Jets," *AIAA Journal*, Vol. 38, No. 4, 2000, pp. 628-635.

[12] Thurow, B., Hileman, J., Samimy, M., Lempert, W., "An In-Depth Investigation of Large Scale Structures in a Mach 1.3 Axisymmetric Jet," AIAA Paper 2001-0148.

[13] Clemens, N. T. and Mungal, M. G., "Large-scale Structure and Entrainment in the Supersonic Mixing Layer," *J. Fluid Mech,* Vol. 284, pp. 171-216, 1995.

[14] Clemens, N. T. and Paul, P. H., "Scalar Measurements in Compressible Axisymmetric Mixing Layers," *Physics of Fluids*, Vol. 7, 1995.

[15] Brown, G. L. and Roshko, A, "On Density Effects and Large Structure in Turbulent Mixing Layers," *J. Fluid Mech.*, Vol. 64, pp. 775-816, 1974.

[16] Jackson, T. L. and Grosch, C. E., "Inviscid Spatial Stability of a Compressible Mixing Layer," *J. Fluid Mech.*, Vol. 28, pp. 609-622, 1989.

[17] Day, M. J., Reynolds, W. C. and Mansour, N. N., "The Structure of the Compressible Reacting Mixing Layer: Insights from Linear Stability Analysis," *Phys. of Fluids*, Vol. 10, pp. 993-1007, 1998.

[18] Hileman, J. and Samimy, M., "Turbulence Structures and the Acoustic Far Field of a Mach 1.3 Jet," AIAA Journal, Vol. 39, No. 9, pp. 1716-1727, 2001.

[19] Kerechanin, C., Samimy, M. and Kim, J.-H., "Effects of Nozzle Trailing Edge Modifications on the far-field acoustic Radiation in Supersonic Jets," AIAA Journal, Vol. 39, No. 6, pp. 1065-1070, 2001.

[20] Lempert, W. R., Wu, P. F., Zhang, B., Miles, R. B., Lowrance, J. L., Mastocola, V. J., and Kosonocky, W. F., "Pulse Burst Laser System for High-Speed Flow Diagnostics," AIAA Paper 96-0179.

[21] Lempert, W. R., Wu, P. F., and Miles, R. B., "Filtered Rayleigh Scattering Measurements Using a MHz Rate Pulse-Burst Laser System," AIAA Paper 97-0500.

[22] Wu, P., Lempert, W. R. and Miles, R. B., "MHz Pulse Burst Laser System and Visualization of Shock-Wave/Boundary Layer Interaction in a Mach 2.5 Wind Tunnel," *AIAA J.*, Vol. 38, pp.672- 2000

[23] Elliott, G. S., Samimy, M., and Arnette, S. A., "A Study of Compressible Mixing Layers Using Filtered Rayleigh Scattering," AIAA Paper 92-0175.

[24] Murakami, E. and Papamoschou, D., "Mixing Layer Characteristics of Coaxial Supersonic Jets," AIAA Paper 2000-2060.

[25] Wainner, R. T. and Seitzman, J. M., "Flow Evolution Measurements from Planar Image Analysis," AIAA Paper 95-1972.

[26] Thurow, B., "Development and Application of a MHz-rate Imaging System on the Visualization of

Turbulence Structure in a Mach 1.3 Axisymmetric Jet," M.S. Thesis, The Ohio State University, 2001.
[27] Smith, K. M. and Dutton, J. C., "A Procedure for Turbulent Structure Convection Velocity Measurements Using Time-Correlated Images," *Exp. in Fluids*, Vol. 27, pp. 244-250, 1999.
[28] Bourdon, C. J. and Dutton, J. C., "Planar Visualizations of Large-Scale Turbulent Structures in Axisymmetric Supersonic Separated Flows," *Physics of Fluids*, Vol. 11, pp. 201-213, 1999.